Multi-Resolution Visualization Techniques for Nested Weather Models

Lloyd A. Treinish
IBM Thomas J. Watson Research Center
Yorktown Heights, NY
lloydt@us.ibm.com

ABSTRACT

Scaling of simulations challenge the effectiveness of conventional visualization methods. This problem becomes two-fold for mesoscale weather models that operate in near-real-time at cloud-scale resolution. For example, typical approaches to vector field visualization (e.g., wind) are based upon global methods, which may not illustrate detailed structure. In addition, such computations employ multi-resolution meshes to capture small-scale phenomena, which are not properly reflected in both vector and scalar realizations. To address the former, critical point analysis and simple bandpass filtering of wind fields is employed for better seed point identification for streamline calculations. For the latter, an encapsulation of nested computational meshes is developed for general realization. It is then combined with the seed point calculation for an improved vector visualization of multi-resolution weather forecasting data.

CR Categories and Subject Descriptions: I.3.8 [Computer Graphics Applications], I.6 [Simulation and Modeling], J.2 [Earth and Atmospheric Sciences]

Additional Keywords: flow visualization, multi-resolution, visualization design, meteorology, weather forecasting.

1. INTRODUCTION

In many applications of simulation, underlying computational grids are defined to capture greater detail in regions of interest. Such grids may focus on different components of complex geometry (e.g., portions of an airframe for a computational fluid dynamics problem) or spatial subdomains for which additional information is to be computed. Independently, they may be fixed or adaptive. The visualization of data defined on such grids is growing in importance as these computational techniques are more widely employed. In addition, visualization of fluid flow continues to be an active research area. Both scalar and vector field visualization are necessary in a specific application domain, that of simulations of weather phenomena. These atmospheric models typically employ a grid that is fixed for a specific computation, but is composed of multiple or nested domains to provide a focus on specific geographic areas.

Our previous work has discussed methods of appropriate mapping of user goals to the design of pictorial content by considering both the underlying data characteristics and the (human) perception of the visualization [8]. However, the introduction of multi-resolution grids challenges the effectiveness of conventional visualization methods. Consider, for example, rapid execution (e.g., 10 to 30 times faster than real-time) of mesocale weather models operating at cloud-scale resolution. Earlier we illustrated that there is a mismatch between this rate of data generation and the ability to utilize the model results with traditional two-dimensional techniques [7]. Three-dimensional visualization is only a partial solution because typical methods can easily fail to capture the salient characteristics of such simulations.

2. PROBLEM

A generalization of our earlier work implies that the resolution of the visualization must match that of the scale of the model to build usable products that are perceptually coherent. The choice of realization geometry is also affected by the resolution of the data so that perceptual artifacts do not dominate the presentation, especially in animation [8]. For typical mesoscale weather models, these issues manifest themselves in two ways. The first is with realization of computed wind fields. The second occurs when visualizing data defined on multi-resolution meshes inherent in the simulation.

2.1 Vector Field Realization

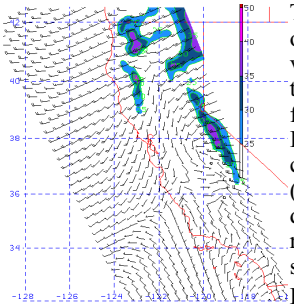

The choice of realization methods is particularly important for vector fields. Figure 1 illustrates the typical method used for operational forecasting tasks. It employs a family of categorical glyphs marked by speed (barbs). This technique is designed for a static display of a relatively small number of fixed samples.

Figure 1. Typical glyph-based visualization of forecast winds.

When used with high-resolution model data, it introduces incorrect motion perception during animation. In addition, subsampling of the original data for glyph locations does not capture the detailed features from the computational grid.

2.2 Nested Grids

The underlying time-varying three-dimensional data are defined on a set of topologically regular, but geometrically irregular meshes. For the geographic area where weather is being forecast, a low-resolution mesh is defined, which is curvilinear horizontally (derived from a cartographic projection). Within that area, one or more high-resolution meshes are imposed to cover areas of interest in greater detail or where expected phenomena of smaller spatial (and temporal) scale will occur. Figure 2 illustrates one of many ways that such a nest configuration could be defined. In this case, there are three nests that focus on the center of the overall domain. The physical spacing between mesh points is in a 4:1 ratio from one grid to the next (i.e., 256:16:1 ratio in areal coverage for three nests). The illustrated meshes are reduced in resolution so that staggering between the nests is visible, following a scheme within the simulation to avoid boundaries artifacts in the computation. Vertically, all of the meshes are the same -- deformed to follow the irregularity of the local terrain. Data are usually defined on the vertices of the mesh. Typical visualizations only consider a single mesh independently of the number or level of nesting or are applied after a uniform resampling of the multiple nests to a single mesh.

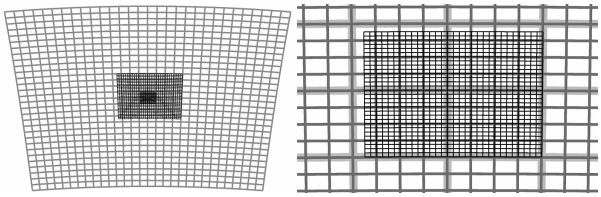

Figure 2. Three-way staggered nesting in a weather model grid.

3. APPROACH

We have determined that realization needs to be based upon the integration of all computational nests with high-resolution topography in a three-dimensional cartographic coordinate system and sequencing consistent with the internal time step of the computation.

3.1 Vector Field Realization

We have used several techniques for wind velocity to avoid problems inherent in traditional barb-based methods. In general, we pseudo-color the realization by speed. For ground level or upper air layers, we typically drape the results over a topographic or another relevant surface to incorporate high-resolution information that strongly affects the model results [8]. A continuous colormap is used ranging from a deep violet or green, for example, for very calm winds to white for the maximum speed. Such a luminance-based colormap is perceptually isomorphic for these data with relatively high spatial frequency [4]. Vector arrows are a common alternative to barbs, but we create them with fixed size to eliminate misleading motion cues during animation as illustrated in Figure 3. It shows the result of a mesoscale forecast generated at 6.5 km resolution in a region roughly 650 x 650 km in extent to include Hawaii. These and subsequent forecast results were generated by the Regional Atmospheric Modeling Systems (RAMS) [3]. Similar issues as discussed herein would apply to other mesoscale models.

The image shows a terrain map as a deformed surface, pseudo-colored by color-filled contour bands of predicted temperature overlaid with coastline maps. This approach generates a textured field, which is effective at showing gross predicted atmospheric movement. The visualization is consistent with prevailing wind patterns in Hawaii. However, this structure is disturbed on the lee side of the big island of Hawaii and to a lesser extent, Maui. These areas are well correlated with warmer areas off the coasts of these islands. Since this realization technique is global in nature, it does not capture sufficient details to interpret these apparent features. Of course, the particular design choices enable a superior representation for the entire forecasting domain compared to either barbs or conventional arrow glyphs, especially for browsing or assessment purposes.

For more detailed examination of these areas, we introduce streamlines with directional arrows. Although visually more complex they are superior at capturing fronts, convergence zones, vortices, etc. An example result for the same forecast period is shown in Figure 4. The temperature data are now shown as a continuous field as better contrast with the wind visualization. A perceptually isomorphic colormap is used between opposing saturation pairs for such low-spatial frequency data. The results show more fine structure, but there are gaps, especially in potentially interesting regions as implied in Figure 3. The problem is that a conventional approach toward steady-state streamline generation was used. In particular, the domain was uniformly sampled to define seed points for integration. While generic, it fails to capture salient high-resolution features. This is a well-known issue in flow visualization, particularly in aerospace computational fluid dynamics and continues to be an active area of research. A key problem in these applications is the understanding of the topology of the underlying vector field, first identified by Helman and Hesselink [2]. Among the more important characteristics of the topology are the location of critical points (i.e., where the velocity field vanishes) and tangent curves, which connect these points. To first order these points can be classified by considering the eigenvalues of the Jacobian of the wind velocity, $\mathbf{v}(u,v)$ as shown in Equation (1), where (x_{cp}, y_{cp}) is the location of a critical point.

$$\left.\frac{\partial(u,v)}{\partial(x,y)}\right|_{(x_{cp},y_{cp})} = \left.\begin{bmatrix} \frac{\partial u}{\partial x} & \frac{\partial u}{\partial y} \\ \frac{\partial v}{\partial x} & \frac{\partial v}{\partial y} \end{bmatrix}\right|_{(x_{cp},y_{cp})} \quad (1)$$

This yields six possible conditions, which are illustrated in Figure 5. In general, this implies that potential regions of interest may be identified by the eigenvectors and eigenvalues of $\mathbf{r} \cdot \mathbf{v}$. In particular, a sampling of the locations where $\mathbf{r} \cdot \mathbf{v} = 0$ is used as a set of (x_{cp}, y_{cp}). These approximate critical points can then be used as seeds for streamline integration.

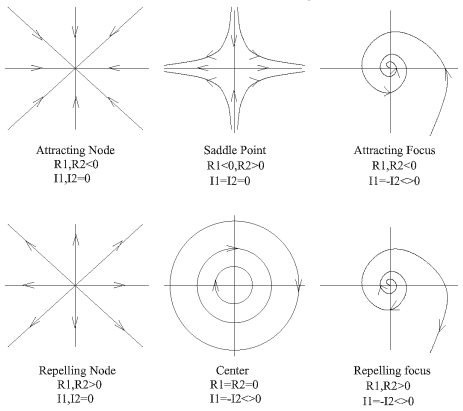

Figure 5. Classification criteria for critical points. R1, R2, and I1, I2 are the real and imaginary components.

The resultant streamlines are thus, a rough approximation of tangent curves. However, there are alternative approaches to determining better locations for streamline seeds. For example, Turk and Banks developed a set of strategies for more optimal streamline placement, which also includes changing locations and lengths, adding to avoid gaps and merging them to avoid crowding [10]. One part of their approach includes iteratively comparing low-bandpass-filtered images of streamlines to evaluate the quality of the streamline placement.

Although we start with a set of seed points derived from critical point analysis, following some of Turk and Banks' ideas, we then apply a bandpass filter to the entire forecasted velocity field as opposed to an image of a streamline representation. This is a simple image-processing approach, which isolates areas of relatively large change in wind speed. The result is complementary seed point locations, which are also used to calculate streamlines. To ensure consistency in this steady-state calculation for animation, both types of seed points are determined for each time step produced by the weather model. An application of this approach for the previous forecast period is shown in Figure 6.

The technique is clearly superior at capturing detailed features from the forecast. In this case, the structure of the wind field on the lee side of the islands is now clear. This morphology is due to vortex shedding of the fluid flow past mountains not unlike what can happen behind a wing or an engine nacelle for a jet aircraft in flight. The results are particularly compelling when animated by time. However, when the time step between animations frames is sufficiently small (i.e., 10 minutes for forecasts at this spatial scale), this approach captures incoherence in the location of the critical points. The resultant animations show some noise or jitter in regions of rapidly changing flow, which detract from both the visual appearance as well as the ability to study the data in detail. This may be an artifact of using a low-order approximation in determining critical point location and thus, similar to the problem recently reported by Scheuermann et al [5]. They argue

for the need to do C^1-scalar interpolation to avoid computing too many and erroneous critical points, and yield a more accurate representation of the topology. Nevertheless, this method looks promising for the visualization of other high-resolution orographic effects on predicted winds.

The techniques described above have been implemented with Visualization Data Explorer (DX) [1]. DX is a portable, general-purpose software package for visualization and analysis. A generic toolkit was used to avoid having to implement a graphics and computational infrastructure. The built-in vector field visualization tools were employed for realization. The critical point analysis was added to DX and the results were then used by the provided streamline calculations.

An improved initial representation of predicted winds enables one to identify features of potential interest for further analysis. We have introduced several additional approaches to study the data in greater detail. The first is to incorporate both spatial and temporal integration as streaklines. Another is to examine other predicted fields generated by the model in conjunction with wind data. Figures 7 and 10 show examples of the latter, fusing multiple variables into a consistent representation [8]. Figure 7 contains results for the same forecast period as used in Figures 3, 4 and 6. It illustrates a surface variable (precipitable water) for display as pseudo-colored filled contour bands, which are overlaid on a topographic map. Coastlines (black) are draped on the surface. An upper air variable (relative humidity) is displayed via surface extraction. The surface at 90% is requested in translucent white, which corresponds roughly to a cloud boundary. Another field (vertical wind speed) has been selected to show as a vertical slice, which is pseudo-color contoured. The location of the slice was chosen to include the area at the lee of Hawaii as identified in Figure 6.

The upper air wind data can be seen along two vertical profiles, which are specified interactively to study this area. The direction of the model wind field along these "virtual soundings" is shown via vector arrows and streamribbons. Both the arrows and ribbons are pseudo-colored by horizontal wind speed. The length of the arrows also corresponds to the horizontal speed. Points along the profile are used as seeds for the streamribbon integration. Each profile is realized as a pseudo-colored tube, which is contoured by the variable selected for isosurface realization (i.e., relative humidity). The visualization for the profile marked "**2**" can help illustrate the upper air characteristics of the predicted vortex shedding described earlier.

3.2 Nested Grid Encapsulation

To enable visualization of data on the staggered nested grids described earlier, the concept of functional access to data was employed [9]. In this case, the unified DX data model was extended to encapsulate nests as a specialization of its native support for multi(zone) grids. This enables any realization method to be utilized to provide results for a single nest or any combination thereof, in the same way one would with a simpler data set. This includes the aforementioned strategy for determining seed point locations for streamline calculations.

Details of the boundaries between nests as well as areas of overlap are hidden from the user. This includes a byte component indicating if a higher-resolution nest exists for an area covered with a lower-resolution nest, which is used to "invalidate" the latter. To enable continuity between the nests in subsequent visualizations, a boundary region is constructed between the perimeter of each inner mesh and the non-overlapping interior vertices of the corresponding outer mesh. In addition to preserving the original grid locations, this approach retains the topological regularity of each of the nests. As a result it is conservative on memory usage and can leverage algorithms that operate on simple structured grids. Since the mesh structure is fixed through the forecast, this encapsulation is only computed once, with the time-varying data being replaced for each simulation step.

There is an additional complication for wind velocity, $\mathbf{v}(u,v)$, for both single and multiple nests. The location of the horizontal (2-vector) component of the velocity is not on the same grid locations, where other (scalar) fields are calculated in the simulation. They are offset from the mesh vertices such that the north-south component (u) are at the same latitude as the other data but half way between longitudes. Similarly, the east-west component points (v) are at the same longitude as the other data but half way between the latitudes. In both cases, the shifting is toward the southwest, but is also encapsulated within this abstraction, which simplifies the application of different realization strategies for the forecasted winds independently of nesting.

A result of these direct operations on the native grids without transformation or compression is preservation of the data fidelity during visualization. Figure 8 illustrates an application of this encapsulation on a scalar, two-dimensional field. In this case, a forecast model was implemented for the northwestern United States, centered on Portland, Oregon. Using the nesting illustrated in Figure 2, meshes at 16, 4 and 1 km between grid points were defined. Each individual nest is a 62x62 grid with 31 vertical levels. Figure 8 shows the topography of this region for each nest integrated as a colored shaded deformed surface, which this technique provides. The boundaries between the nests have been marked with a gray, translucent box draped over the surface.

Similar computational grid structures do occur in other disciplines. For example, Schulz et al reports on visualization methods for locally-refined cartesian grids used for fluid flow calculations [6]. However, the meshes in this case are not staggered while they are geometrically regular and the refinement is always the same in each dimension. Hence, issues of encapsulation and realization are much simpler than for those of weather simulations discussed herein.

4. RESULTS

The nesting, critical point analysis and image-based seed point selection methods are combined to visualize actual forecast results and evaluate the techniques. Figure 9 uses methods for both surface and upper air data described earlier. In this case, the inner two nests (4 and 1 km resolution, respectively) for the aforementioned Portland forecasts are shown using the nest encapsulation discussed earlier. The image shows contours of surface temperature and streamlines of surface winds that are draped over the (nested) model topography. The temperature predictions are interpolated to the locations of cities of interest within the geographic area and the results are marked on the terrain. Two volumetric upper air fields are also shown via translucent isosurfaces. Total cloud water density at 10^{-3} kg/kg (water/air) is visible in white. Predicted reflectivities at 30 dbZ corresponding to where precipitation is forming is shown in cyan. Additional detail for the 1 km resolution mesh in the center can be seen, especially for the surface data. In animation of a 48-hour forecast at 10 minutes per time step, the streamlines show lateral jittering likely due to the aforementioned approximation in the critical point analysis. However, they do capture the flow along the Columbia River Gorge reasonably well even in the lower-resolution nest and certainly better than with the previously used uniform seeding strategy for streamlines.

Figure 10 shows another approach in which four different surface variables have been selected in a combined visualization at the same time as in Figure 9. Temperature is shown as pseudocolor. Wind velocity is illustrated as streamlines, colored by speed, using the same technique as in Figures 6 and 9. Colored line contours of relative humidity in increments of 10% are shown. Each of these planar representations are deformed vertically by maximum reflectivity to create a shaded surface. The data for each of these realizations is using the two inner nests integrated together using the same approach as in Figure 9. Additional detail for the 1 km resolution mesh can be seen in each of the variables. For geographic context, coastline (black), state boundary (white) and river (blue) maps are draped on the surface. Regions of higher reflectivity implying precipitation are correlated with those of higher humidity. One can also see streamlines corresponding to the area of the Columbia River Gorge as illustrated in Figure 9. In animation, the jitter in this representation for the streamlines is no longer visible because the time steps are separated by one hour. This suggests a threshold in temporal sampling for this resolution forecast when higher order methods are required for critical point determination.

These techniques provide more detailed and consistent visualizations then those typically used with such weather simulations. Since conventional meteorological visualizations only show individual nests, they would fail to illustrate the more detailed nests in geographic context of the simulation as in Figures 9 and 10. In addition to only showing single nests, such visualizations would usually employ glyph-based methods as in Figure 1 or more rarely streamlines. But the latter would be based upon uniform sampling of the nest. In either case, the detailed structure in the forecast winds would not be adequately portrayed in the visualization.

5. Conclusions and Future Work

Encapsulation of complex meshes coupled with critical point analysis and image-based seed point placement on flow data defined on such structures enables the generation of useful visualizations that capture the detail of the underlying simulation. Further adaptation of on-going work in flow visualization looks promising in applications to high-resolution numerical weather models. As the complexity of the underlying meshes increases to accommodate orographic and other effects in detail, the encapsulation method will be tested. Additional techniques for improved global representation such as line integral convolution will be utilized.

For animations with fine temporal resolution, either higher-order methods for critical point determination or some time-averaging of the solution to $\mathbf{r} \cdot \mathbf{v} = 0$ will be applied to eliminate incoherence in streamline positions between frames. Additional image-based approaches will be considered, including extension of some of the ideas developed by Turk and Banks. For more detailed investigation, the critical point analysis will be used for tangent curve classification. This may indicate more precisely regions of separation or attachment of predicted wind fields. It could also be used to identify seeds to illustrate specific types of flows (e.g., vortices) as part of more focused visualizations.

6. Acknowledgements

The author wishes to thank F. Suits and Z. Christidis of IBM T. J. Watson Research Center for valuable discussions on techniques and issues on the visualization of and computation on nested grids.

7. References

[1] Abram, G. and L. Treinish. *An Extended Data-Flow Architecture for Data Analysis and Visualization*. **Proceedings of the IEEE Visualization 1995 Conference**, October 1995, Atlanta, pp. 263-270. (DX is now available as open source software via `http://www.research.ibm.com/dx` and `http://www.opendx.org`).

[2] Helman, J. L. and L. Hesselink. *Surface Representations of Two- and Three-Dimensional Fluid Flow Topology*. **Proceedings of the IEEE Visualization 1990 Conference**, October 1990, San Francisco, pp. 6-13.

[3] Pielke, R., W. Cotton, R. Walko, C. Tremback, W. Lyons, L. Grasso, M. Nicholls, M.-D. Moran, D. Wesley, T. Lee and J. Copeland. *A Comprehensive Meteorological Modeling System - RAMS*. **Meteorol. Atmos. Phys.**, **49**, 1992, pp. 69-91.

[4] Rogowitz, B. and L. Treinish. *Data Visualization: The End of the Rainbow*. **IEEE Spectrum**, **35**, no.12, December 1998, pp. 52-59.

[5] Scheuermann, G., Z. Tricoche and H. Hagen. *C1-Interpolation for Vector Field Topology Visualization*. **Proceedings of the IEEE Visualization 1999 Conference**, October 1999, San Francisco, pp. 271-278.

[6] Schulz, M., F. Reck, W. Bertelheimer, T. Ertl. *Interactive Visualization of Fluid Dynamics Simulations in Locally Refined Cartesian Grids*. **Proceedings of the IEEE Visualization 1999 Conference**, October 1999, San Francisco, pp. 413-416.

[7] Treinish, L. and L. Rothfusz. *Three-Dimensional Visualization for Support of Operational Forecasting at the 1996 Centennial Olympic Games*. **Proceedings of the 13th IIPS Conference**, February 2-8, 1997, Long Beach, pp. 31-34.

[8] Treinish, L. *Task-Specific Visualization Design*. **IEEE Computer Graphics and Applications**, **19**, n. 5, September/October 1999, pp. 72-77.

[9] Treinish, L. *A Function-Based Data Model for Visualization*. **Proceedings of the IEEE Visualization 1999 Conference Late Breaking Hot Topics**, October 1999, San Francisco, pp. 73-76.

[10] Turk, G. and D. Banks. *Image guided streamline placement*. **Computer Graphics, Proceedings of ACM SIGGRAPH '96**, August 1996, New Orleans, pp. 453-460.

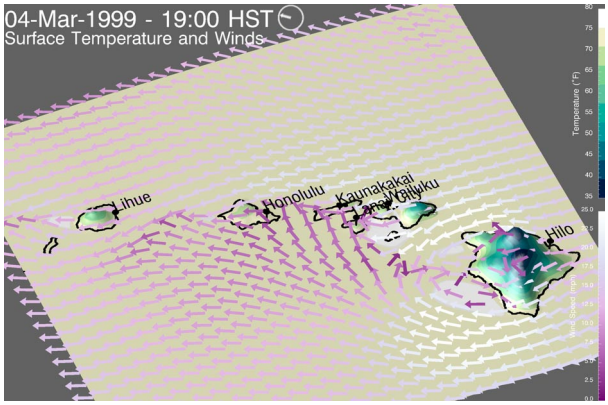

Figure 3. Predicted winds visualized as arrow glyphs with temperature contours and a terrain surface.

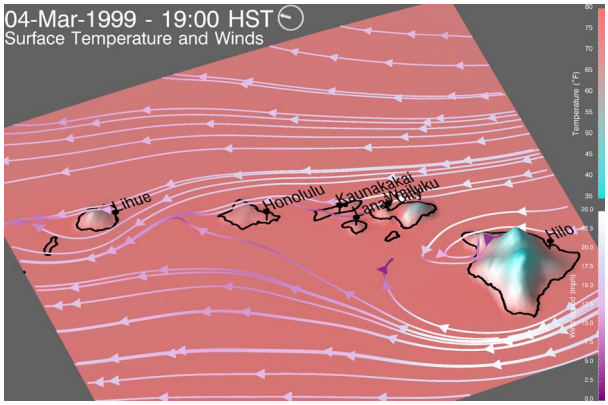

Figure 4. Predicted winds visualized as streamlines with a terrain surface colored by temperature.

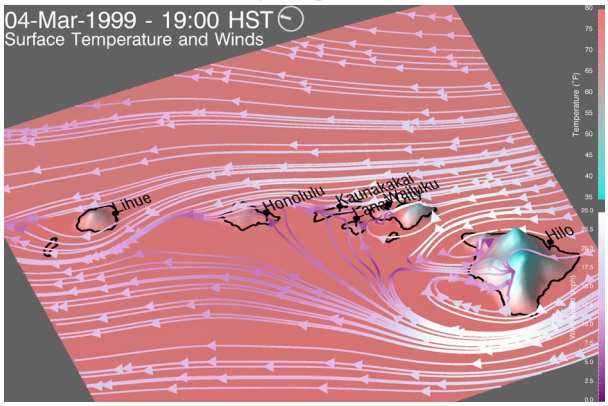

Figure 6. Wind streamlines from seeds selected by critical point analysis supplemented with image-based guidance.

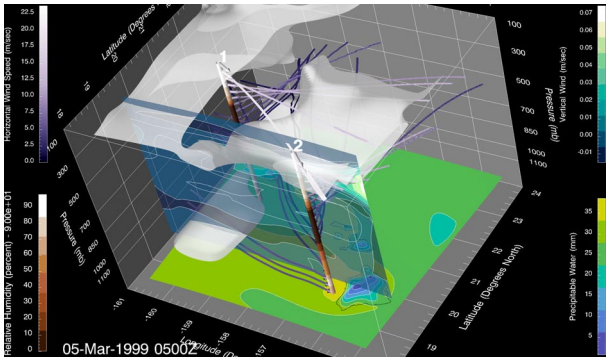

Figure 7. Three-Dimensional Wind Streamlines with Surface and Upper Air Data.

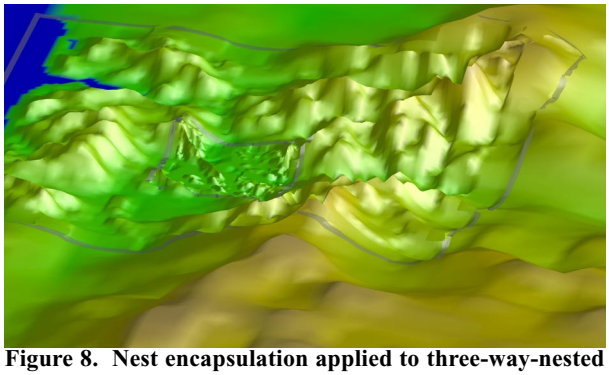

Figure 8. Nest encapsulation applied to three-way-nested model topography.

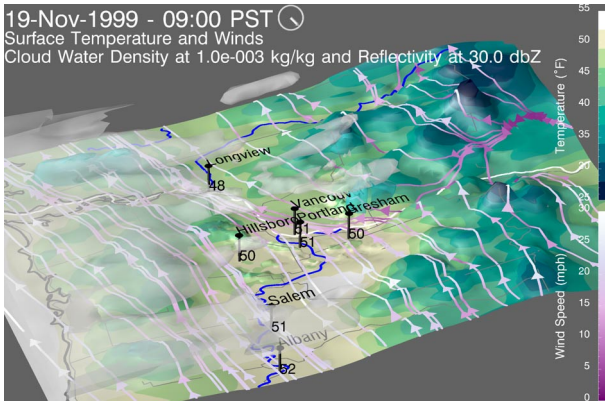

Figure 9. Integration of wind streamlines with other surface variables and upper air data on two nests. The streamlines are derived from seeds selected by critical point analysis supplemented with bandpass-filtering on the velocity field to identify areas of relatively large change in wind speed.

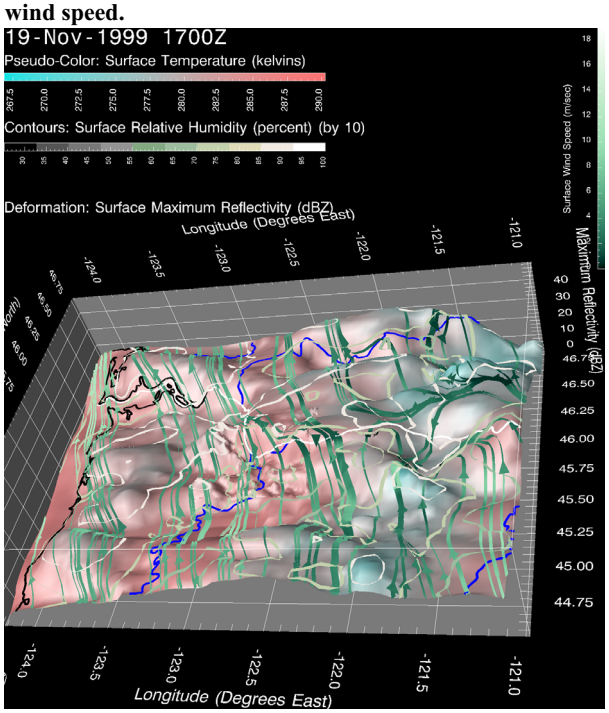

Figure 10. Integration of wind streamlines with other surface variables on two nests. The streamlines are derived using both techniques for seed point identification.